HYDROSTATIC JOURNAL BEARINGS

Summary

In a hydrostatic bearing an external source of pressurized fluid forces lubricant between two surfaces; thus enabling non-contacting operation and the ability to support a load. Hydrostatic bearings can support large loads without journal rotation and provide large (accurate and controllable) direct stiffness as well as damping (energy dissipation) coefficients.

Hydrostatic bearings rely on external fluid pressurization to generate load support and a large centering stiffness, even in the absence of journal rotation. The load capacity and direct stiffness of hydrostatic bearings do not depend on fluid viscosity, thus making them ideal rotor support elements in process fluid pumps. Current applications intend to replace oil lubricated bearing with hybrid bearings to improve efficiency with shorten rotor spans and less mechanical complexity. Current cryogenic liquid turbopumps implement hydrostatic bearings enabling an all fluid film bearing technology with very low number of parts and no DN limit operation. Details on the bulk-flow analysis of turbulent flow hydrostatic bearings are given along with the discussion of performance characteristics, static and dynamic, for hydrostatic bearings supporting a water pump. Angled liquid injection produces a hydrostatic bearing with unsurpassed dynamic force and stability characteristics.

Introduction

Hydrostatic bearings derive their load capacity not from shear flow driven effects (hydrodynamic wedge and surface sliding) but rather from the combination of pressure versus flow resistance effects through a feed restrictor and in the film lands. Figure 1 depicts thrust and radial hydrostatic bearing configurations for process fluid lubrication turbopumps. Table 1 presents the major advantages and disadvantages of hydrostatic bearings.

Fig 1. Hydrostatic radial and thrust bearings for process fluid rotating machinery

The hydrostatic stiffness is of unique importance for the centering of high-precision milling machines, gyroscopes, large arena movable seating areas, telescope bearings, and even cryogenic fluid turbo pumps for rocket engines. Note that hydrostatic bearings require an external pressurized supply system and some type of flow restrictor. Also, under dynamic motions, hydrostatic bearings may display a pneumatic hammer effect due to fluid compressibility. However, and most importantly, the load and static stiffness of a hydrostatic bearing are independent of fluid viscosity; thus making this bearing type very attractive for application with non-viscous fluids, including gases and cryogens.

Table 1. Hydrostatic Bearings: Advantages and Disadvantages

Advantages	Disadvantages
Support very large loads. The load support is a function of the pressure drop across the bearing and the area of fluid pressure action.	Require ancillary equipment. Larger installation and maintenance costs.
Load does not depend on film thickness or lubricant viscosity.	Need of fluid filtration equipment. Loss of performance with fluid contamination.
Long life (infinite in theory) without wear of surfaces	High power consumption because of pumping losses. Potential to induce hydrodynamic instability in hybrid mode operation.
Provide stiffness and damping coefficients of very large magnitude. Excellent for exact positioning and control.	Potential to show pneumatic hammer instability for highly compressible fluids, i.e. loss of damping at low and high frequencies of operation due to compliance and time lag of trapped fluid volumes.

Consider the fundamental operation of a simple one dimensional hydrostatic bearing [Rowe 1983, San Andrés 2002]. The flow is laminar and fluid inertia effects are not accounted for; i.e. a classical lubrication example. Figure 2 depicts a 1D bearing of very large width (B). A hydrostatic bearing combines two flow restrictions in series, one at the feed or supply port, and the other through the film lands. In the feed restrictor (orifice, capillary, etc.) the fluid drops its pressure from the supply value (P_s) to a magnitude (P_R) within a recess or pocket of typically large volume (see Figure 3). Since the recess is deep, the pocket pressure is regarded as uniform over the entire recess area $A_R=bB$. The fluid then flows from the recess into the film lands of small thickness h, and discharges to ambient pressure through the bearing sides, say $P_a=0$ for simplicity.
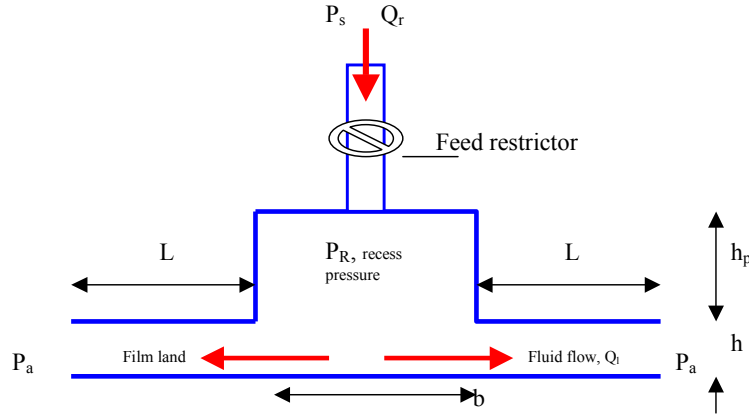
Fig. 2 Geometry of a simple 1-D hydrostatic bearing

The flow rate (Q_r) across the restrictor is a function of the pressure drop, $Q_t = f(P_s - P_R)$. For an orifice and capillary feeding,

$$Q_r = Q_o = A_o C_d \sqrt{\frac{2}{\rho}(P_s - P_R)} \quad ; \quad Q_r = Q_c = \frac{\pi d^4}{128 \mu \ell_c}(P_s - P_R) \tag{1}$$

with A_o and C_d as the orifice area and empirical discharge coefficient, respectively. (d, ℓ_c) are the diameter and length of the capillary tube, typically $\ell_c \gg 20\, d$. The orifice coefficient (C_d) ranges from 0.6 to 1.0, depending on the flow condition (Reynolds number), the orifice geometry and even the film thickness. Under turbulent flow conditions, tests and CFD analysis evidence $C_d \sim 0.80$.

Across the bearing film lands the fluid drops in pressure from (P_R) to ambient pressure, P_a. In the laminar flow of an incompressible fluid, the flow rate is a function of the pressure drop and equals

$$Q_\ell = -\frac{B h^3}{12\mu}\frac{\partial P}{\partial x} = +\frac{B h^3 (P_R - P_a)}{12 \mu L} \tag{2}$$

where B is the bearing width and L is the film length with thickness h. Presently, no surface motion along the x-axis is accounted for, i.e. the bearing is stationary. Under steady state conditions, the flow through the restrictor equals the flow through the film lands, i.e.

$$Q_r = f(P_s - P_R) = 2 C_l (P_R - P_a) = 2 Q_l \tag{3}$$

with $C_l = B h^3/(12 \mu L)$ as a flow-conductance along the film land. Eqn. (3) permits the determination of the recess pressure (P_R) given the film conductance (C_l) and feed restrictor parameters. For bearing design, a value of pocket pressure (P_R) is desired, and Eqn. (3) serves to size the diameter of the supply restrictor.

For the simple bearing considered, the pressure field on the bearing surface takes the shape shown in Figure 3. Note that the recess pressure is assumed uniform or constant

within the pocket extent (*b*). The assertion is not valid for flows with large Reynolds numbers (highly turbulent), shallow pockets and with large journal rotational speeds. The film pressure generates a reaction force,

$$F = B \int P(x)dx = B\left\{ P_R \frac{L}{2} + P_R b + P_R \frac{L}{2} \right\} = B(L+b)P_R \tag{4}$$

where $P_a=0$ for simplicity. The force (*F*) is proportional to the recess pressure (P_R) and the area B $(L + b)$. Note that, in the absence of surface relative motion, **a hydrostatic bearing has a limit load capacity, $[B(L+b)]P_s$.**
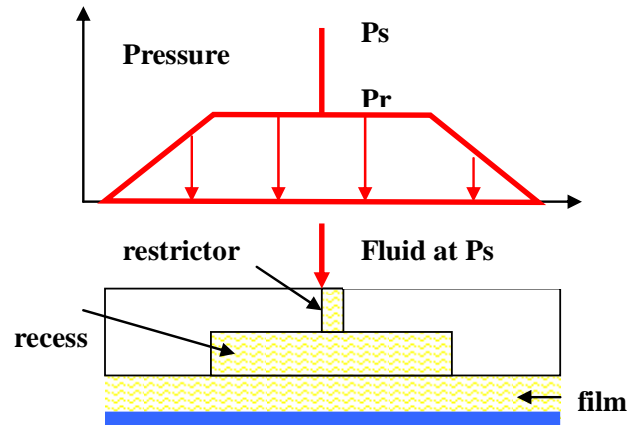

Fig. 3 Pressure profile in a simple 1-D hydrostatic bearing

A static change in film thickness ($h_0+\Delta h$) with $\Delta h \ll h_0$, causes the recess pressure to change to $P_{Ro} +\Delta P_R$, since the flow conductance varies. $\Delta P_R <0$ as $\Delta h>0$. Integration of the change in pressure gives rise to a the hydrostatic stiffness K

$$K = -\frac{\Delta F}{\Delta h} = \frac{3B(L+b)}{h_o} \frac{P_{Ro}}{(Z+1)} \tag{5}$$

with $Z = Z(P_{Ro}) = \dfrac{(P_{Ro} - P_a)}{a(P_s - P_{Ro})}$, $a = 2$ for orifice or $a = 1$ for capillary feed. The hydrostatic stiffness is proportional to the bearing area $[B(L+b))$, the recess pressure (P_{Ro}), and inversely proportional to the film thickness (h_o). Most importantly, the stiffness is not an explicit function of fluid viscosity. Figure 4 depicts the dimensionless stiffness,

$$\overline{K} = \frac{K \cdot h_o}{3B(L+b)P_s} = \frac{p_{ro}}{Z+1} \tag{6}$$

versus recess pressure ratio, $p_{ro}=P_{Ro}/P_s$, for bearings with orifice and capillary feeds, respectively. Hydrostatic bearings with orifice compensation have larger stiffness than capillary fed bearings. Orifices are usually preferred since their diameters are larger than those of capillaries. This is important since restrictor clogging may cause catastrophic

bearing failure, unless a micron size filtering device is used as part of the fluid feed (supply) system into the bearing.
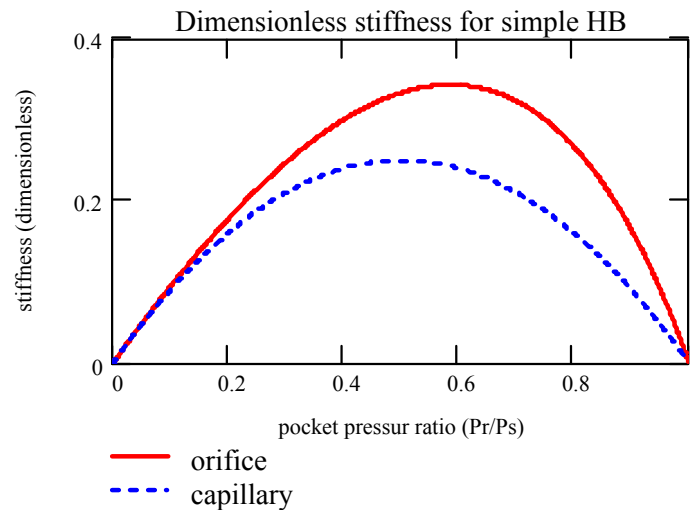
Dimensionless stiffness for simple HB

Fig. 4 Static stiffness for simple hydrostatic bearing (laminar flow w/o fluid inertia effects, incompressible fluid)

A maximum (optimum) hydrostatic stiffness occurs for a given recess pressure p_{ro}. For a capillary p_{ro}=0.500, while for an orifice p_{ro}=0.5857. In a capillary fed hydrostatic bearing, the pressure drops across the restrictor should match the pressure drop across the film lands. The optimum stiffness arises from an impedance matching between the feed restrictor and the flow resistance through the film lands. In the figure, a low value of recess pressure indicates a large flow resistance (small conductance) through the restrictor, while a large recess pressure denotes a large flow resistance through the film lands.

In sum, hydrostatic bearings with orifice restrictors offer larger stiffness than with capillary restrictors. The bearing direct stiffness depends on the pocket pressure (< supply pressure) and does not dependent explicitly on lubricant viscosity. Without an external pressure supply and restrictor, there is no stiffness or load support.

Effects of excitation frequency, pocket volume, and fluid compressibility on the dynamic force coefficients of a hybrid bearing

The analysis above explains the physics for the generation of support stiffness in a simple hydrostatic bearing configuration. The stiffness derived is static, strictly valid for low frequency motions. Motions at other frequencies produce notable changes in both the stiffness and damping force coefficients. Fluid compressibility within the recess volume and surface velocity (hydrodynamic effects) must be accounted for in a hybrid bearing (combination hydrostatic / hydrodynamic).

The conservation of mass within the recess of a hydrostatic bearing balances the flow through the restrictor (Q_r), the flow into the film lands $(2Q_l)$ and the time rate of change of fluid mass accumulated within the pocket,

$$Q_R - 2Q_l = \frac{1}{\rho} \frac{\partial(\rho V_{rec})}{\partial t} \tag{7}$$

where $V_{rec} = B\, d(h + h_R)$ is the recess volume, $h(t)$ is the film thickness, and h_R is the machined pocket depth. The density and pressure in a compressible liquid are related through the material bulk-modulus κ, i.e. $d\rho = \frac{\rho}{\kappa} dP$.

Let the film thickness h be the superposition of a steady-state value (h_0) and a harmonic motion of small amplitude Δh and frequency (ω), i.e.

$$h = h_0 + \Delta h \cos(\omega t) = h_0 + \Delta h\, e^{i\omega t}\,; \text{ and } \dot{h} = i\,\omega\, \Delta h\, e^{i\omega t} \tag{8}$$

Note that,

$$\frac{1}{\rho} \frac{\partial(\rho V_{rec})}{\partial t} = \left(V_{rec_0} \frac{P_{R_l}}{\kappa} + A_{rec} \right) i\,\omega\, \Delta h\, e^{i\omega t} \tag{9}$$

with $V_{rec_0} = A_{rec}(h_0 + h_R)$. Eqn (9) shows that the fluid mass in the pocket volume varies dynamically with changes in film thickness and pocket pressure, thus introducing a pressure-lag effect which can induce undesirable dynamic force effects, namely *pneumatic hammer* with generation of a "negative" damping coefficient. Introducing a *break frequency (ω_B)* [San Andrés 1991]

$$\omega_B = \frac{Q_{r_0}}{P_{R_0}} \frac{(Z+1)\kappa}{V_{rec_0}} = (Z+1) \frac{\kappa}{V_{rec_0}} \frac{h_0^3 B}{6\mu L} \tag{10}$$

Note that $\omega_B \to \infty$ for an incompressible fluid ($\kappa \to \infty$). A lengthy algebraic analysis leads to the following expressions for <u>frequency dependent</u> force coefficients [San Andrés 1991],

$$K_{(\omega)} = K_0 \frac{\left(1 + \dfrac{f^2}{\alpha} \right)}{\left(1 + f^2 \right)}\,;\quad C_{(\omega)} = C_0 \frac{(1 - \alpha)}{(1 + f^2)} \tag{11}$$

where $f = \dfrac{\omega}{\omega_B}$ is a frequency ratio, $\alpha = \dfrac{K_o}{\omega_B C_o}$ is a **damping loss** ratio; and (K_0, C_0) are the stiffness and damping coefficients for an incompressible fluid, i.e. one without liquid compressibility ($\kappa \to \infty$),

$$K_0 = \frac{3\,B(L+b)}{h_0}\,\frac{P_{R_0}}{(Z+1)}; \quad C_0 = \frac{6\,\mu\,B\,L(L+b)^2}{h_0^3}\,\frac{1}{(Z+1)} \qquad (12)$$

with $Z = Z(P_{Ro}) = \dfrac{(P_{R_0} - P_a)}{a(P_s - P_{R_0})}$. Note that the <u>static</u> stiffness coefficient (K_0) is directly proportional to the recess pressure (P_R). On the other hand, the "static" damping coefficient (C_0) depends solely on the fluid viscosity and the bearing area, and it grows rapidly as the film thickness (h) decreases. Incidentally, the surface speed (U) does not aid to the generation of force coefficients in laminar flow hydrostatic bearings.

Figure 5 depicts the hydrostatic bearing stiffness (K) and damping (C) coefficients for increasing excitation frequency ratios (ω/ω_B). The results correspond to a bearing with a deep pocket depth $(h_R/h=10)$ and damping loss factor $(\alpha=0.42)$ typical of a LH2 application. In general, the hydrostatic stiffness increases as the excitation frequency grows while the damping coefficient drops dramatically. See [San Andrés 1991] for a more detailed analysis with examples related to cryogenic fluid hydrostatic bearings.
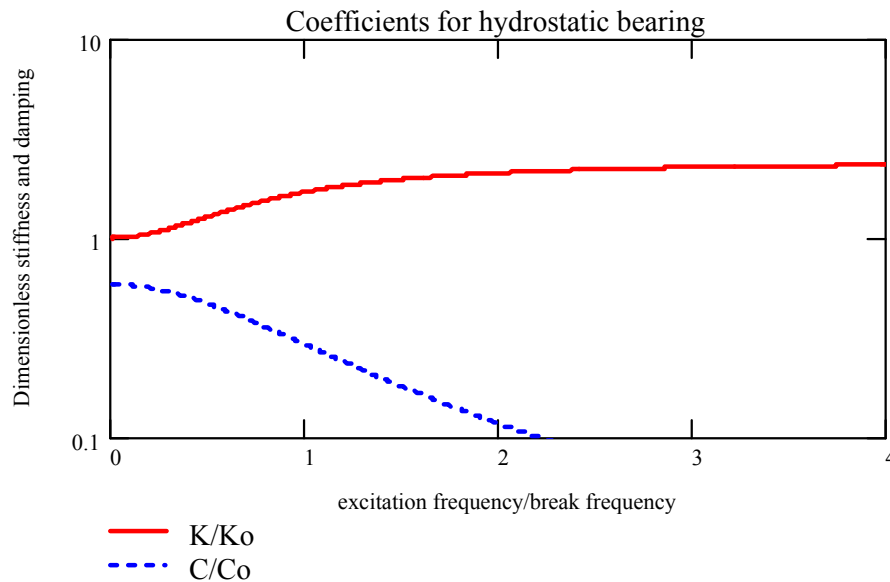

Fig. 5 Effect of excitation frequency on the (dimensionless) direct stiffness and damping force coefficients of a simple hydrostatic bearing

For excitations at low frequencies, $\omega \rightarrow 0$ $(\omega \ll \omega_B)$,

$$K_{(\omega=0)} \rightarrow K_0 \;; C_{(\omega=0)} \rightarrow C_0(1-\alpha) \qquad (13)$$

there is a loss of damping due to fluid compressibility effects $(\alpha>0)$. This reduction may cause the bearing to become unstable even under static conditions if $\alpha >1$. This phenomenon, known **as pneumatic hammer,** is characteristic of gas hydrostatic bearings

with feed pockets. Fir stability purposes, gas hydrostatic bearings avoid pockets or volumes, using feed holes impinging directly on the bearing surface.

For excitations at large frequencies, ($\omega \to \infty$, $\omega >> \omega_B$),

$$K_{(\omega \to \infty)} = K_\infty = \frac{K_0}{\alpha} \quad ; \quad C_{(\omega \to \infty)} = 0 \tag{14}$$

there is a complete loss of damping accompanied by an increase in dynamic stiffness. For excitations at a frequency coinciding with the break frequency (ω_B), the stiffness and damping coefficients are

$$K_{(f=1)} = \frac{1+\alpha}{2\alpha} K_o \quad ; \quad C_{(f=1)} = \frac{1}{2} C_{(f=0)} = \frac{1}{2} C_o (1-\alpha) \tag{15,16}$$

Thus, the damping coefficient is just 50% of the value obtained at low frequencies.

The force coefficients are frequency independent in a nearly incompressible fluid ($\kappa \to 0$, $\omega_B \to \infty$). However, even in commonly assumed incompressible liquids, the fluid bulk modulus decreases rapidly with minute (volume) concentrations of dissolved gases.

To reduce **fluid compressibility effects** (*avoid loss of damping*) it is desirable to design the hydrostatic bearing with a break frequency (ω_B) as high as possible, and/or to operate the bearing under dynamic conditions with excitation frequencies well below the break frequency, i.e. $f<<1$.

From Eqn. (10), to increase the break frequency, large values for the following ratio are needed,

$$\left(\frac{h_0^3 B}{V_{rec_0}} \frac{1}{6L} \right) = \left(\frac{h_0^2}{6dL} \frac{1}{\left[1 + \dfrac{h_R}{h_0} \right]} \right) >> 1 \tag{17}$$

That is, deep pockets ($h_R/h_0 >> 1$) tend to aggravate the loss of damping at low excitation frequencies.

It is notable to mention that the whirl frequency ratio for a centered hybrid bearing is

$$\phi = WFR = \frac{K_{XY}}{\Omega C_{XX_{f=0}}} = \frac{K_{XY}}{\Omega C_{XX_{=0}} (1-\alpha)} \approx 0.5 \frac{1}{(1-\alpha)} \tag{18}$$

Hence, hybrid bearings (combination hydrostatic – hydrodynamic) show the same limited whirl frequency ratio as plain cylindrical bearings. This ratio could even be worse, *WFR > 0.5* if $\alpha > 0$, i.e. if fluid compressibility –recess volume effects are important.

Modern applications of hydrostatic bearings
The importance of hybrid (combination hydrostatic and hydrodynamic) journal and thrust bearings and damping seal bearings as radial support elements cryogenic turbomachinery

has steadily grown. Compact - low count part turbo pumps operate sub critically at exceedingly high shaft speeds (> 100 krpm) and delivering pressures as large as 550 bar. Advanced primary power require of externally pressurized fluid film bearings to support the expected large thrust and lateral radial loads.

Hybrid journal bearings (HJB) enable smaller and lighter turbopumps through no bearing DN life limitation and sub critical rotor operation, i.e. at speeds below the first elastic mode of the rotor-bearing system. HJBs offer durability, low friction and wear, accuracy of positioning, and large direct stiffness and damping force coefficients. These features enable the design (and operation) of un-shrouded impellers with a significant increase in the turbopump mechanical efficiency. The growth of an "all-fluid-film- bearing" technology for advanced and less costly (per launch cost) turbopumps demands the development of analytical models and design tools, the testing of components, and the implementation of the technology [San Andrés, 1990, 1995, 1997].

Note that for the cryogenic fluid application as well as others handling low viscosity liquids, the large surface speeds and the large pressure differential determine flow conditions with high levels of flow turbulence and fluid inertia effects. Flow turbulence increases the lubricant "effective" viscosity, thus enhancing the load capacity due to hydrodynamic effects and increasing the bearing energy dissipation characteristics, i.e. more damping. Computational programs based on the Reynolds equation of classical lubrication, i.e. no fluid inertia, are ill-prepared to render adequate predictions of hybrid bearing performance, static and dynamic force coefficients.

Bulk flow analysis of turbulent flow hydrostatic bearings

Comprehensive computational analyses for prediction of the static and dynamic forced response of process fluid hybrid bearings, radial and thrust, are available [San Andrés, 1990-2000]. The analyses address to the most important theoretical and practical issues related to the operation and dynamic performance of cryogenic fluid film bearings, i.e. geometric configuration, operating conditions, flow turbulence, fluid inertia, realistic fluid properties, thermal effects, and two-phase flow phenomena. Extensive test measurements were conducted to benchmark the predictive codes. A brief overview of the physical model for the fluid flow in hydrostatic bearing follows.

Figure 6 shows the geometry of a hybrid (combination hydrostatic/hydrodynamic) journal bearing. A liquid at high pressure (P_s) is supplied through orifice restrictors and impinges into the bearing recesses with a mean pressure (P_R). The fluid injection is typically radial; though in some instances it could be at an angle opposing shaft rotation. Angled injection aids to reduce the development of the fluid flow circumferential speed and reduce, even eliminate, the cross-coupled stiffness force coefficients.
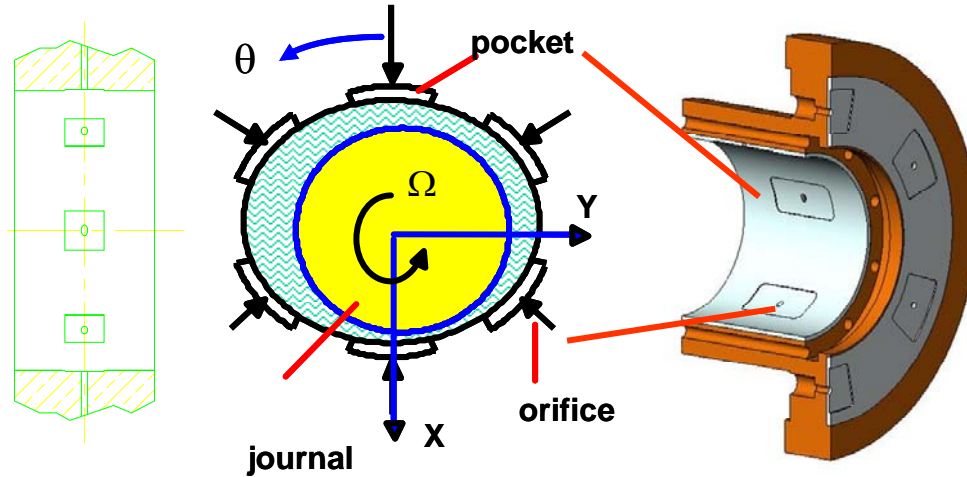
Fig 6. Schematic views of a radial hydrostatic/hydrodynamic journal bearing

The computational model considers the fully developed turbulent bulk-flow of a fluid whose material properties depend on its local thermo physical state of pressure and temperature. The general transport equations including these features are [San Andrés 1995]:

$$\frac{\partial(\rho h \psi)}{\partial t} + \frac{\partial(\rho h V_x \psi)}{\partial x} + \frac{\partial(\rho h V_z \psi)}{\partial z} = S \qquad (19)$$

where	Variable	Source term, S
conservation of mass equation	$\psi = 1$	0
transport of circumferential *(x)* momentum velocity	$\psi = V_x$	$-h\frac{\partial P}{\partial x} - \frac{\mu}{h}\left(\kappa_x V_x - \kappa_J \frac{\Omega R}{2}\right)$
transport of axial momentum *(z)* velocity	$\psi = V_z$	$-h\frac{\partial P}{\partial z} - \frac{\mu}{h}\left(\kappa_z V_z\right)$

Above *(V_x, V_z)* are the buk-flow (film averaged) circumferential and axial flow velocities, P is the pressure, and *(κ_x κ_z)* denote wall shear stress turbulent flow coefficients. The wall shear stress parameters $\kappa_y = \kappa_x = \frac{1}{2}(\kappa_J + \kappa_B)$ with $\kappa_J = f_J Re_J$, $\kappa B = f_B Re_B$, and the friction factors *($f_{J,B}$)* depend on the bearing and journal surface conditions and the flow Reynolds numbers relative to the rotating (Re_J) and stationary (Re_B) surfaces.

The pressure field within the bearing pockets or recesses is determined from flow continuity with the film lands, momentum exchange at the orifice plane and a viscous rise due to journal rotation. As shown in Fig. 7, at the recess edges, an inertial pressure drop also occurs due to the sudden transition from the recess of depth (h_R) into the film lands of thickness (h). Past the recesses, the liquid then flows through the film lands and the pressure drops to the discharge value (P_a).

Consider a recess with axial length (l) and circumferential extent (b). The recess area (A_R) equals (lxb) and the feed orifice has diameter d_o with a feed volume equal to V_{supply}. CFD predictions and measurements show the generation of hydrodynamic pressures within the pocket, followed by sharp inertial pressure drops at the recess edges [San Andrés 1990, 1995].
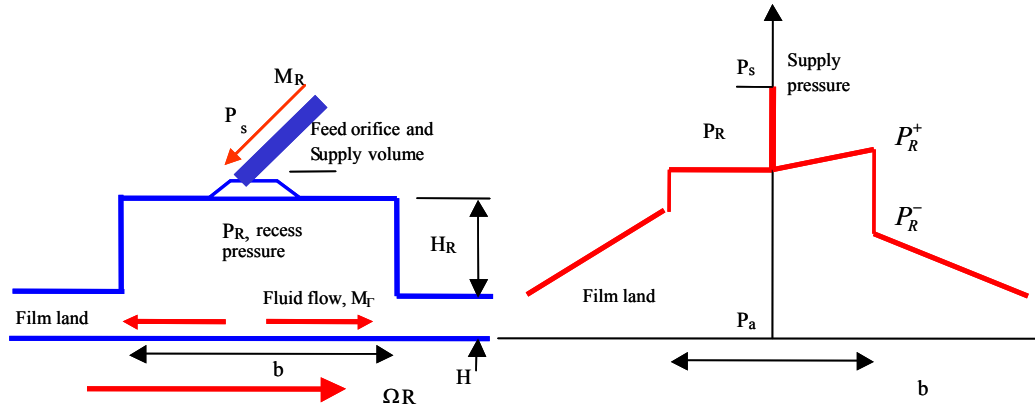

Fig. 7. Turbulent flow pressure distribution in a pocket of a hybrid bearing

The continuity equation at a hydrostatic recess establishes a balance among the mass flow through the feed orifice (M_R), the flow through the boundaries of the recess into the film lands (M_Γ), and the accumulation of fluid mass within the recess volume, $V_R=[A_R (h+h_R)+V_{supply}]$. That is,

$$M_R = C_d\, A_o \left(\frac{\rho}{2}\left[P_s - P_R \right] \right)^{1/2} = M_\Gamma + \frac{\partial}{\partial t}\left(\rho V_R \right)$$

(20)

where $A_o = C_d\,(\pi d_o^2/4)$ is the effective orifice area, and $M_\Gamma = \oint_\Gamma \left(\rho\, h\, \vec{V} \cdot \vec{\eta} \right) d\Gamma$ is the outflow from the pocket into the bearing film lands. The circumferential pressure downstream of the feed orifice, P_R^+, is given, as in a Rayleigh step bearing]

$$P_R^+ = P_R + \mu\, \kappa_x\, \frac{b}{2\left(h+h_R \right)^2} \left\{ \frac{\Omega R}{2} - V_x \right\}_R$$

(21)

Fluid inertia causes a sudden pressure drop at the interface between a recess and the film lands. The fluid pressures, P_R^-, entering into the film lands bounding a recess are

$$P_R^- = P_R^+ + \frac{(1+\xi)}{2}\rho\left[1-\left(\frac{\rho_e^-}{\rho_e^+} \right)\left(\frac{h}{h+h_R} \right)^2 \right] V_{x,z}^2$$

(22)

where (ξ) represents empirical entrance loss coefficients at the recess edges, axial and circumferential. The sudden pressure drop is accounted for only if the fluid flow effectively enters into the thin film lands.

San Andrés and Childs [1997] extend the bulk-flow model to account for fluid injection at an angle and opposing shaft rotation. This design feature retards the full development of the circumferential flow velocity, thus reducing the cross-coupled stiffness coefficients which prevent the operation of hybrid bearings at large rotational speeds. San Andrés [2007] presents time transient response predictions during the start-up of a cryogenic turbopump to determine the lift-off speed of the rotor on its hydrostatic bearings.

Example of hydrostatic bearings for load support in a water pump

The design of a water hydrostatic bearing to replace a mineral oil lubricated bearings in a multiple stage water pump follows. The hydrostatic bearing size, length and diameter, see Table 2, are similar to the original bearing to reduce costs in redesigning or re-machining the pump casing and shaft (journal). The pressurized water feeding the hydrostatic bearing is routed from the pump discharge volute. Eliminating the lubrication system offers distinct advantages, including better system performance, lower operational cost, and extended periods for maintenance.

Table 2: Geometry and operating conditions of a water lubricated hydrostatic bearing

Diameter, D=Length, L = 152. 4 mm
Nominal clearance, c =0.102 mm,
5 pockets: axial length l=51 mm, arc 41° , depth=0.381 mm
Orifice diameter: 3.2 mm (C_d=0.80)
Smooth bearing and rotor surfaces
Fluid: water at 30°C (0.792 cPoise, 995 kg/m^3)
Nominal speed = 3600 rpm, Supply pressure= 34.4 bar

Note that L/D=1, D/c=1,465. The ratio of pockets area to bearing area, (L x D), equals 0.19, and the pocket depth to clearance ratio is 3.75. The pocket area is relatively small to avoid excessive flow rate requirements. The pockets are shallow to reduce the likelihood of pneumatic hammer effects and to enhance hydrodynamic effects at the pocket ends. Hydrostatic bearings with reduced pocket areas (< 25 % of bearing area) and shallow pockets are modern considerations relying on the desired adequate dynamic forced performance of the bearing.

The design analysis considers the bearing operating without an applied load at its centered position, i.e. null eccentricity. Figure 8 shows the bearing flow rate and drag power increasing as the orifice diameter is enlarged since the pocket pressure increases. The bearing flow rate is 1.67 kg/s (~100 liter/min), which is large when compared to the requirements of an oil-lubricated bearing, yet not large enough to cause a severe reduction in pump available flow rate (~ 4% pump flow routed to bearings). At the nominal speed of operation (3.6 krpm), the size of the orifice is selected to provide the maximum direct (support) stiffness while keeping a low flow rate to avoid a penalty on pump performance.

HJB design: At nominal operating condition Ps-Pa=34.4 bar, 3600 rpm   L=D=0.152 m, **c=102 um,** 5 pocket (l=L/3, arc =42 deg)

Drag power (kW)

Flow rate (kg/s)

Supply pressure

Recess pressure ratio

selected orifice diameter

Pocket pressure ratio
HJB flow rate (kg/s)
Power (kw)

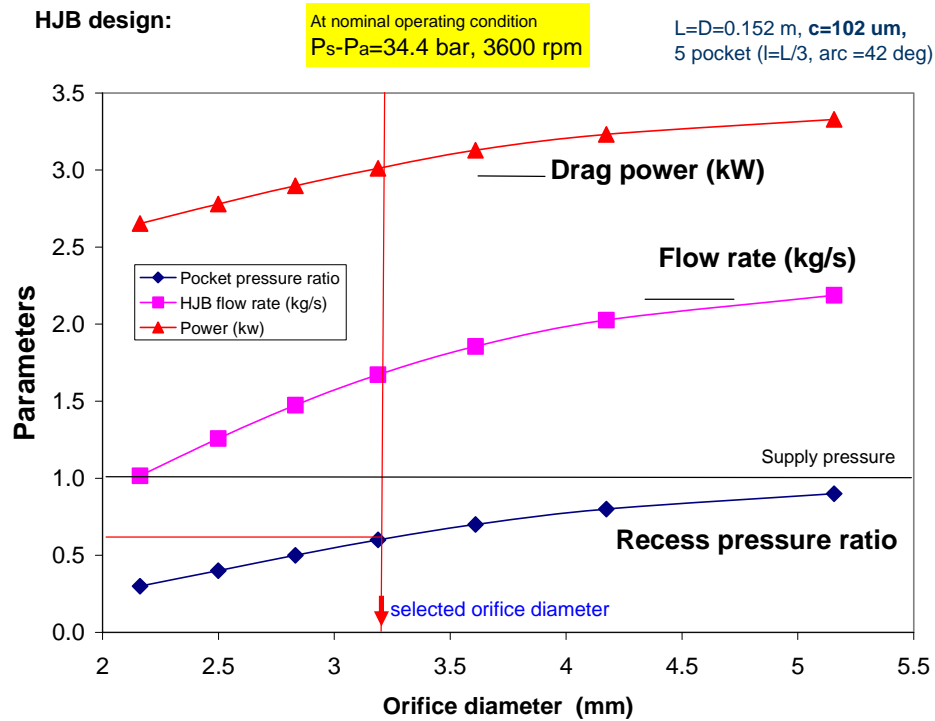Parameters

Orifice diameter (mm)

Fig. 8 Performance parameters for water hydrostatic bearing: pocket pressure, flow rate and drag power versus orifice diameter. Nominal centered operating condition

Figure 9 depicts the stiffness coefficients, direct (K_{XX}) and cross-coupled (K_{XY}), versus the pocket pressure ratio. The direct stiffness peaks at a pocket pressure ratio ~ 0.60 which requires an orifice of diameter equal to 3.20 mm. The magnitude of direct stiffness equals 350 MN/m, which is large enough to support the static load of 5 kN with a relatively small rotor eccentricity. Note that the cross coupled stiffness is about 50% lower than the direct stiffness, thus indicating journal rotation hydrodynamic effects will affect greatly the bearing dynamic forced performance.

HJB design:

At nominal operating condition
Ps-Pa=34.4 bar, 3600 rpm

L=D=0.152 m, **c=102 um,**
5 pocket (l=L/3, arc =42 deg)

Kxx = Kyy

$Kxx - Mxx\,\omega^2$

Kxy = -Kyx

Stiffness coefficients

- Kxx (MN/m)
- Kxy (MN/m)
- Kxx-Mxx w^2

3.20 mm
Selected orifice diameter
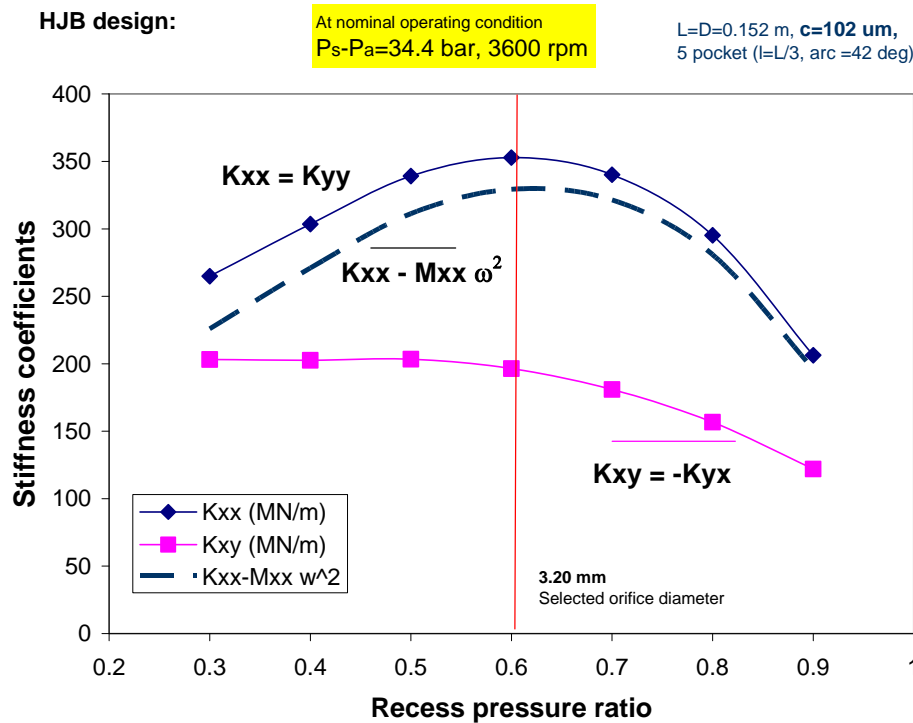
Recess pressure ratio

Fig. 9 Direct and cross-coupled stiffnesses versus recess pressure ratio for water hydrostatic bearing. Nominal centered operating condition (no load)

Figure 10 presents the viscous damping (C_{XX}, C_{YX}) and fluid inertia (M_{XX}, M_{YX}) force coefficients decreasing with the recess pressure ratio (and also with the size of the feed orifice). The added mass coefficient is ~ 166 kg at the selected orifice diameter. In spite of the large mass predicted, its effect on reducing the direct dynamic stiffness is relatively small, as seen on Figure 8 in the (K_{XX} - $M_{XX}\,\omega^2$) curve. The direct damping coefficients are large due to flow turbulence conditions; however, the cross-coupled stiffness coefficients are also large. Thus, the whirl frequency ratio[1], $WFR = K_{XY}/(C_{XX}\,\omega)$, is ~0.60. This too restrictive stability indicator could easily prevent the implementation of the water bearing into the pump application. To resolve this issue, a modification with angled fluid injection directed against shaft rotation is recommended. See [San Andrés, 2006] for

---

[1] The onset and persistence of severe (large amplitude) sub synchronous vibrations at rotational speeds above a certain threshold speed evidences a hydrodynamic instability in rotor-fluid film bearing systems that is due to the effect of journal rotational speed in the shear induced flow field. This condition is typical of fixed geometry bearings. The threshold speed corresponds to the rotor speed at which a bearing loses its effective damping, and any small perturbation from an equilibrium position will determine unbounded rotor motions. The whirl frequency ratio (*WFR*) denotes the ratio between the onset whirl frequency (typically the system first critical speed) and the threshold speed of instability. Plain journal bearings show a *WFR* equal to 0.50 for small to moderate operating eccentricities (light loads), and thus instability onsets at rotational speeds equal to twice the system first critical speed. Measurements in hybrid bearings verify closely the prediction of *WFR* =0.50. In some circumstances the *WFR* even increases above 0.50, in particular for low rotational speeds and large supply pressures

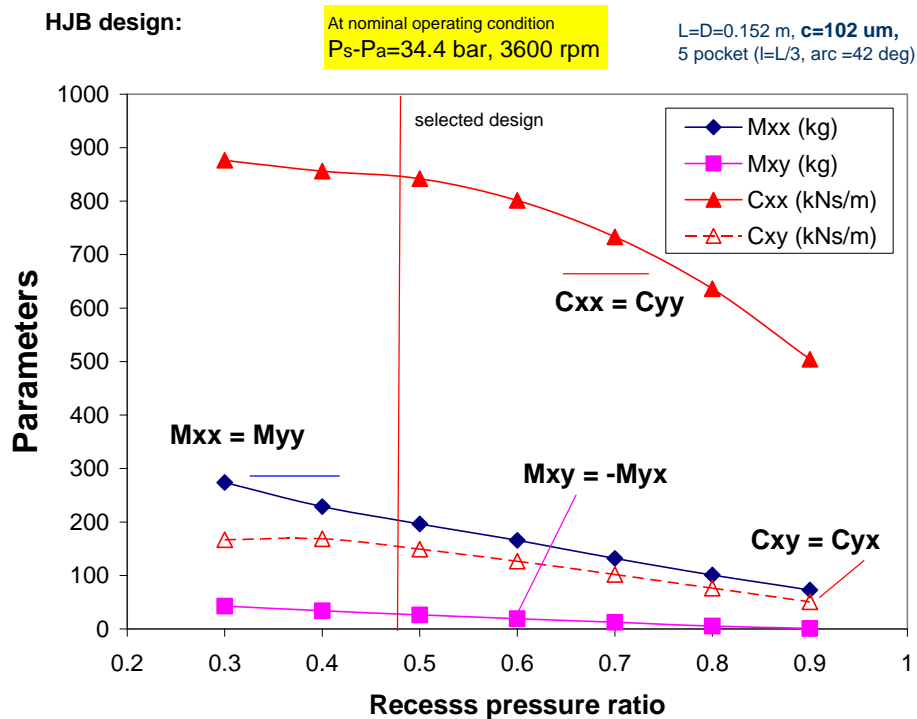details on the water hydrostatic operation with a load of 5 kN and for speeds ranging from 1krpm to 5 krpm.

HJB design:

At nominal operating condition
$P_S-P_a=34.4$ bar, 3600 rpm

L=D=0.152 m, **c=102 um,**
5 pocket (l=L/3, arc =42 deg)

Fig. 10. Damping and inertia force coefficients versus recess pressure ratio. Nominal centered operating condition

Closure

Modern high performance turbomachinery operating at high speeds and large pressures incorporate process fluid hybrid (hydrostatic/hydrodynamic) journal and thrust bearings to reduce the numbers of parts and size, and to eliminate expensive mineral lubricant storage and pumping, thus further satisfying stringent environmental constraints.

Despite the many advantages offered by hydrostatic bearings, rotordynamic instabilities due to hydrodynamic (shear flow) and fluid compressibility effects are issues of primary concern for high speed operation with large pressure differentials. Pneumatic hammer effects are avoided by appropriate selection of the flow restrictor, by designing bearing recesses with small volumes, and by restricting bearing operation to flow conditions where the pressure differential is a small fraction of the liquid bulk modulus.

Fixed geometry hydrostatic bearings have limited stability characteristics with a whirl frequency ratio (*WFR*) ~0.50, as in plain hydrodynamic journal bearings. The 50% frequency whirl condition limits severely the application of hydrostatic bearings to high speed, light weight and flexible rotating machinery. Concerted efforts have been directed towards conceiving hybrid bearings with improved stability characteristics, and without

loss in centering stiffness and damping ability. Some of the technological advances evolved from analysis and engineering design, while others followed empiricism and well known past experiences.

The recommended fixes to improve the hydrodynamic stability of hydrostatic bearings by reducing or eliminating the whirl frequency ratio (*WFR*) are:

a) Use textured bearing surfaces to decrease the cross-coupled stiffness coefficients. Test results with a knurled-pattern HJB show a *WFR* as low as 0.30 but with a reduced load capacity and direct stiffness when compared to a smooth surface HJB [Franchek et al., 1995]

b) Use angled liquid injection opposing journal rotation to reduce the development of the circumferential flow velocity leading to a virtual elimination of cross-coupled stiffness coefficients [San Andrés and Childs, 1997]. Measurements conducted on a five-pocket water hydrostatic bearing verify the analysis, demonstrating that angled injection aids in reducing the whirl frequency ratio without decreasing the bearing centering stiffness and load capacity. However, the effectiveness of angled injection is reduced as shaft speed increases towards high values where shear flow driven effects overcome the hydrostatic effect.

c) Introduce geometrical changes in the bearing to induce a stiffness orthotropy. For example, circumferentially asymmetric grooved bearings can produce large anisotropy on the rotordynamic force coefficients [San Andrés, 2001]. This design enhances stability by rendering a lower direct stiffness in the plane of the axial grooves as compared to the orthogonal stiffness. Measurements have demonstrated the enhancement in performance.

d) Implement flexure pivot-tilting pad hydrostatic bearings [San Andrés and Zhu, 2007, San Andrés et al. 2008], see Figure 11. These bearings are mechanically complex though nearly free of instabilities, i.e. the pads support flexibility eliminates the generation of cross-coupled stiffnesses. This type of bearing with air as the lubricant has shown wondrous potential for ready implementation in high-speed micro turbomachinery.
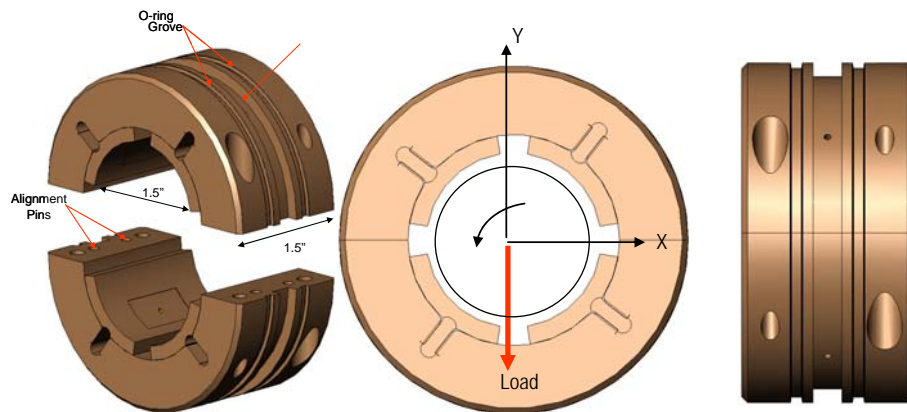

Fig. 11. Flexure pivot hydrostatic bearing for high speed turbomachinery

Extensive analytical and experimental research has brought forward the technology of hybrid journal bearings for advanced cryogenic turbo pump and process fluid applications. Computational analyses accounting for flow turbulence, fluid inertia and compressibility, and thermal effects are available to bearing designers and rotordynamics engineers. Laboratory measurements of load, leakage and torque, and identification of rotordynamic force coefficients aided to benchmark the computational model predictions.

References

WB Rowe, Hydrostatic and Hybrid Bearing Design, Butterworths, (1983).

San Andrés, L., Fluid Compressibility Effects on the Dynamic Response of Hydrostatic Journal Bearings, L. San Andrés, WEAR, (1991), **146**, pp. 269-283

San Andrés, L., Turbulent Hybrid Bearings with Fluid Inertia Effects, ASME Journal of Tribology, (1990), **112,** pp. 699-707.

San Andrés, L., Thermohydrodynamic Analysis of Fluid Film Bearings for Cryogenic Applications, AIAA Journal of Propulsion and Power, (1995), **11,** 5, pp. 964-972.

San Andrés, L., and D. Childs, Angled Injection - Hydrostatic Bearings, Analysis and Comparison to Test Results, ASME Journal of Tribology, (1997), **119**, 1, pp. 179-187.

San Andrés, L., Bulk-Flow Analysis of Hybrid Thrust Bearings for Process Fluid Applications," ASME Journal of Tribology, (2000), **122**, pp. 170-180.

San Andrés, L., Start- up Response of Fluid Film Lubricated Cryogenic Turbo- Pumps, 43rd AIAA/ASME/SAE/ASEE Joint Propulsion Conference & Exhibit, Cincinnati, OH, July 9-11, (2007), Paper AIAA-2007-5093.

San Andrés, L.,, Annular Pressure Seals and Hydrostatic Bearings, Paper 11, von Karman Institute - RTO Lecture Series,   DESIGN AND ANALYSIS OF HIGH SPEED PUMPS, NATO RTO-AVT-143, ISBNs 92-837-0063-5 / 978-92-837-0063-0 (2006).

N. Franchek, D. Childs and L. San Andrés, Theoretical and Experimental Comparisons for Rotordynamic Coefficients of a High-Speed, High-Pressure, Orifice-Compensated Hybrid Bearings, ASME Journal of Tribology, (1995), **117**, 2, pp. 285-290.

San Andrés, L., A Hybrid Bearing with Improved Rotordynamic Stability, 1st International Conference in Rotordynamics of Machinery, ISCORMA1, Paper 2006 (2001).

Zhu,S., and San Andrés, L., Rotordynamic Performance of Flexure Pivot Hydrostatic Gas Bearings for Oil-Free Turbomachinery," Journal of Engineering for Gas Turbines and Power, (2007), **129**(4), pp. 1020-1027.

San Andrés, L., S. Phillips and D. Childs, Static Load Performance of a Hybrid Thrust Bearing: Measurement and Validation of Predictive Tool, 6th Modeling and Simulation Subcommittee / 4th Liquid Propulsion Subcommittee / 3rd Spacecraft Propulsion Subcommittee Joint Meeting, Orlando, Florida, December 8-12, (2008), JANNAF-120 Paper.

Visit URL: http://phn.tamu.edu/TRIBGroup to learn more about research in hydrostatic bearings, radial and thrust, sponsored by industry. Recent work with hydrostatic gas bearings is showcased. The site shows existing test rigs, experimental data and comparisons to model predictions. The site also provides a full list of technical reports and archival papers on hydrostatic bearings (liquid and gas).